



Contents lists available at ScienceDirect



# Catalysis Today

journal homepage: [www.elsevier.com/locate/cattod](http://www.elsevier.com/locate/cattod)

## Three-dimensional 10-ring zeolites: The activities in toluene alkylation and disproportionation

Martin Kubů<sup>a</sup>, Naděžda Žilková<sup>b</sup>, Stacey I. Zones<sup>b</sup>, Cong-Yan Chen<sup>b</sup>, Sulaiman Al-Khattaf<sup>c</sup>, Jiří Čejka<sup>a,c,\*</sup>

<sup>a</sup> J. Heyrovský Institute of Physical Chemistry, Academy of Sciences of the Czech Republic, Dolejškova 3, CZ-182 23 Prague, Czech Republic

<sup>b</sup> Chevron Energy Technology Company, Richmond, CA 94 802, USA

<sup>c</sup> Center of Research Excellence in Petroleum Refining and Petrochemicals, King Fahd University of Petroleum & Minerals, Dhahran 31261, Saudi Arabia

### ARTICLE INFO

#### Article history:

Received 20 March 2015

Received in revised form 14 May 2015

Accepted 19 May 2015

Available online xxx

#### Keywords:

10-ring zeolites

TUN

IMF

-SVR

\*SFV

Toluene alkylation

Disproportionation

### ABSTRACT

Three-dimensional 10-ring zeolites TUN, IMF, -SVR, MFI and MEL were investigated as for their acid properties, adsorption of 2,2-dimethylbutane and in toluene disproportionation and its alkylation with isopropyl alcohol. The results were compared against zeolite \*SFV, the structure of which consists mainly of MEL zeolite with some additional 12-ring channel system. With exception of -SVR synthesized with high Si/Al ratio, all other zeolites provided Si/Al ratios in a narrow region. Novel zeolites TUN, IMF, and -SVR exhibited higher conversions than MFI and MEL in toluene alkylation. TUN and IMF were substantially more active in toluene disproportionation indicating less diffusion restrictions of channel structure on the disproportionation reaction. \*SFV showed a similar catalytic behavior to MEL with much lower selectivity to *p*-xylene and *p*-cymene. This could indicate that both toluene disproportionation and alkylation proceed in reaction space of \*SFV being similar to those of MFI and MEL. \*SFV and TUN exhibited much faster adsorption of 2,2-dimethylbutane than MFI, MEL, IMF, and -SVR. It was concluded that the presence of some larger transport pores in \*SFV than in other zeolites is responsible for fast adsorption of 2,2-dimethylbutane and transport of products resulting in a low selectivity to *p*-xylene and *p*-cymene.

© 2015 Elsevier B.V. All rights reserved.

## 1. Introduction

Transformations of aromatic hydrocarbons represent one of the most important groups of reactions in petrochemical processes [1–3]. Alkylation, disproportionation, isomerization, and transalkylation reactions usually carried out over zeolite catalysts allow upgrading of low value chemicals like benzene or toluene to those of higher practical interest, such as ethylbenzene, *p*-xylene or cumene [4,5]. In this respect, zeolite channel structures and types and concentration of acid sites play the decisive role as for the zeolite activities and selectivities are concerned. In addition to the practical application of zeolites as catalysts in industrial processes, zeolites can serve as model catalysts for investigating reaction mechanisms and structure–acidity–activity relationship for novel zeolites [6–10].

225 different structural types of zeolites were already recognized by the International Zeolite Association [11]. The individual types of zeolites differ in the size of the channels (8-, 10-, 12- or 14-rings), their connectivity and the presence or absence of cages in channel intersections or along the channel itself [12–15]. Zeolite acidity and channel architecture control the activity and selectivity in transformations of organic compounds [7,9,16,17]. In addition to conventional three-dimensional zeolites, novel zeolite morphologies including layered [18–21], pillared [22], self-pillared [23], hierarchical [24,25], or nanospunge [26] zeolites have been also synthesized and their properties described in detail. Activity and selectivity of zeolite catalysts in catalytic reactions are directly related to the structure, texture and chemical composition of a particular zeolite under study.

In this contribution we investigated the relationship among the pore structure of several novel medium-pore zeolites (TUN, IMF, -SVR, \*SFV) and their acidity in toluene alkylation with isopropyl alcohol and in toluene disproportionation. Toluene disproportionation was chosen as one of these reactions because it reflects not only the structural features and acidity of the zeolite catalysts under study, due to the possibility of monomolecular and bimolecular

\* Corresponding author at: J. Heyrovský Institute of Physical Chemistry, Academy of Sciences of the Czech Republic, Dolejškova 3, CZ-182 23 Prague, Czech Republic. Tel.: +420 26605 3795; fax: +420 28658 2307.

E-mail address: [jiri.cejka@jh-inst.cas.cz](mailto:jiri.cejka@jh-inst.cas.cz) (J. Čejka).

**Table 1**

List of zeolites under study and their structural characteristics.

Sample	Reference	Dimensionality of the channels	Type of the channels	Size of the channels (nm)
TUN	[27]	3D	(10+10) × 10	0.55 × 0.60 + 0.52 × 0.60; 0.54 × 0.55
IMF	[28]	3D	10 × 10	0.55 × 0.56; 0.53 × 0.59
-SVR	[29]	3D	10 × 10 × 10	0.55 × 0.57; 0.52 × 0.59; 0.52 × 0.56
*SFV	[17]	3D	12 × 10 × 10	0.51 × 0.82; 0.56 × 0.56; 0.50 × 0.55
MFI		3D	10 × 10	0.51 × 0.55; 0.53 × 0.56
MEL		3D	10	0.53 × 0.54

mechanism, but also the product selectivity for preferential xylene formation [9]. Toluene alkylation provides even more information about the reaction volume and acidity of zeolites due to the parallel alkylation/disproportionation reactions, selectivity to cymenes, *p*-cymene and also a possible formation of secondary products like *n*-propyl toluene requiring a particular channel arrangement [6]. All zeolites were characterized by XRD, adsorption isotherms, SEM, and FTIR spectroscopy with different probe molecules.

TUN, IMF, -SVR, and \*SFV zeolites were recently synthesized and they possess rather complex structures consisting of intersecting 10-rings, their structural features are listed in Table 1. TUN zeolite was synthesized by group of Hong [27]. Structure of zeolite IMF was determined by Baerlocher et al. [28] describing it as two-dimensional system of 10-ring channels with limited third dimension along (010). Unit cell of -SVR zeolite has 24 different crystallographic sites, one of them forms ordered Si vacancy [14,29]. Synthesis of TUN, IMF, and -SVR is carried out using diquaternary alkylammonium ions based on N-methyl pyrrolidine. The only difference among the individual SDAs (structure directing agents) is the length of the carbon chain between two heterocyclic rings. TUN is prepared with 1,4-bis-(N-methyl-pyrrolidinium) butane (1,4-MPB), whereas IMF and -SVR with pentane (1,5-MPP) and hexane (1,6-MPH) analogs, respectively.

## 2. Experimental

### 2.1. SDA preparation

The divalent SDA cations were prepared, purified and characterized as follows:

The synthesis is generally carried out according to Fig. 1. 0.48 mol (20% excess) of N-methyl pyrrolidine (MP, 98% Acros) was mixed with 200 ml of methanol (99+, Acros) and stirred while drop-wise adding of 0.2 mol of 1,*n*-dibromoalkane (*n* = 4–6). Final mixture was stirred at room temperature for 4 days. Unreacted amine and solvent were evaporated, obtained white sediment dissolved in boiling isopropyl alcohol (99.5%, Lachner) and yellowish solution put into the fridge for recrystallization. After 2 days, trituration with acetone (99.5%, Lachner) and its consecutive evaporation to dryness finished the procedure. Due to high sensitivity to moisture, all SDAs were stored closed in a flask before using in the synthesis. The purity was determined by <sup>1</sup>H NMR.

### 2.2. Zeolite synthesis

#### 2.2.1. TUN

TUN zeolite was synthesized from the reaction gel with the following molar composition: 4.5(1,4-MPB-Br<sub>2</sub>)·11Na<sub>2</sub>O·0.75Al<sub>2</sub>O<sub>3</sub>·30SiO<sub>2</sub>·1200H<sub>2</sub>O [27]. Distilled water,

1,4-MPB dibromide, Al(NO<sub>3</sub>)<sub>3</sub>·9H<sub>2</sub>O (p.a., Lachner), NaOH (98%, Lachner) and fumed silica (Aldrich) were mixed together exactly in the written order. Each chemical was added after dissolving the previous ones. After being stirred at room temperature for 1 day, the mixture was transferred to Teflon-lined 500 ml autoclave and heated at 160 °C for 12 days under agitation and autogenous pressure.

#### 2.2.2. IMF

For IMF synthesis [30], the aqueous solution of 1,5-MPP dibromide was prepared. Then NaAlO<sub>2</sub> (52% Al<sub>2</sub>O<sub>3</sub>, 42.5% Na<sub>2</sub>O, Riedel de Haën), NaOH, NaBr (99+, Acros) and fumed silica were added. The mixture with the molar composition 10(1,5-MPP-Br<sub>2</sub>)·17Na<sub>2</sub>O·6NaBr·Al<sub>2</sub>O<sub>3</sub>·60SiO<sub>2</sub>·2400H<sub>2</sub>O was stirred for 2 h to form an uniform gel [31]. Crystallization proceeded in Teflon-lined 25 ml autoclaves at 175 °C for 10 days under static conditions.

#### 2.2.3. -SVR

High silica -SVR zeolite was synthesized in fluoride media in the presence of 1,6-MPH hydroxide [32]. For that purpose, 1,6-MPH dibromide (11.1 g), distilled water (56.1 g) and AG1-X8 resin (28.7 g) were put together and stirred overnight at room temperature for exchanging 1,6-MPH to its hydroxide form. After filtration, 64 g of the obtained solution was mixed with 12.6 g of tetraethyl orthosilicate (TEOS, 98.5%, Aldrich). Water and ethanol formed from TEOS hydrolysis were allowed to evaporate to evident dryness in a hood for 5 days. 0.2 g of LZ-210 zeolite (partially dealuminated Y zeolite) as a potential contributor of aluminum, 0.1 g of as-made pure-silica -SVR as seeds, 3.7 g of distilled water and 1.25 g of 40% HF (p.a., Lachner) were added and stirred with plastic spatula until thick gel was formed. Resulting gel was placed in Teflon-lined stainless steel 25 ml autoclaves and heated at 170 °C under agitation for 9 days.

#### 2.2.4. \*SFV

\*SFV zeolite was synthesized using N-butyl-N-cyclohexylpyrrolidinium hydroxide as a template [33]. The resulting gel in a 25 ml Teflon liner was capped off and placed in a Parr bomb Steel reactor and heated in an oven at 170 °C, while rotating at 43 rpm, for 18 days. The mixture was filtered through a fritted-glass funnel, the obtained solids were washed generously with water, then rinsed with a small amount of acetone and allowed to air-dry overnight and further dried in an oven at 120 °C [17].

#### 2.2.5. MFI

MFI zeolite was purchased from PQ Corporation (CBV-8020) in NH<sub>4</sub>-form with Si/Al = 34.5.

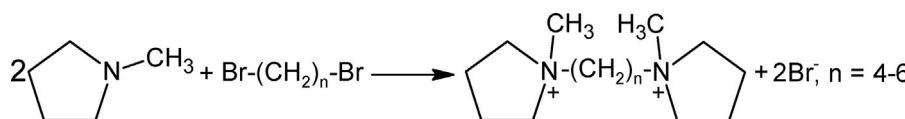


Fig. 1. SDA preparation.

### 2.2.6. MEL

As for MEL zeolite, 51 g of TEOS was slowly added dropwise to the aqueous solution containing 2.6 g of  $\text{Al}(\text{NO}_3)_3 \cdot 9\text{H}_2\text{O}$  and 26 g of distilled water and the solution was stirred for 90 min. Afterwards, NaOH (0.5 g) dissolved in water (21.4 g) was slowly added dropwise. Finally, 31.45 g of tetrabutylammonium hydroxide (40% in  $\text{H}_2\text{O}$ , Fluka) used as a SDA and 34 g of water were quickly added under vigorous stirring and the reaction mixture was stirred for 120 min. The crystallization was carried out under agitation in Teflon-lined 90 ml autoclaves at 170 °C for 6 days.

After synthesis of each zeolite, the autoclaves were immediately cooled down by stream of water, solids recovered by filtration, washed repeatedly with copious amount of distilled water and dried overnight in the oven at 60 °C. The individual zeolites were calcined under flowing air at 580 °C for 12 h with a heating rate of 1 °C/min to remove the organic content. To get ammonium form, calcined samples were four-times treated with 1.0 M  $\text{NH}_4\text{NO}_3$  solution (99%, Lachner) for 4 h each time at room temperature using 100 ml of solution per 1 g of sample. In order to obtain its proton form, calcination at 450 °C for 2 h followed.

Structural characteristics of zeolites under study are given in Table 1.

### 2.3. Characterization

The structure and crystallinity of as-made and calcined samples were checked by X-ray powder diffraction. Patterns of prepared samples were recorded on Bruker AXS D8 Advance equipped with a graphite monochromator and a position sensitive detector Väntec-1 using  $\text{CuK}\alpha$  radiation and para focusing in Bragg-Brentano geometry.

The size and shape of zeolite crystals were examined by scanning electron microscopy (SEM, JEOL, JSM-5500LV). For measurements crystals were coated with a thin platinum layer by sputtering in vacuum chamber of a BAL-TEC SCD-050.

For chemical composition of zeolites X-ray fluorescence analysis (XRF) using a spectrometer Philips PW 1404 provided with an analytical program UniQuant enabling determination of 74 elements from fluorine to uranium. For these measurements samples were mixed with dentacryl as a binder and pressed on the surface of cellulose pellets.

Concentration of Lewis and Brønsted acid sites was determined after adsorption of pyridine by FTIR spectroscopy (Nicolet Protégé 460 Magna with a transmission DTGS and MTC/A detector). Samples were pressed into self-supporting wafers with a density of 8.0–12 mg/cm<sup>2</sup> and activated in situ at 430 °C overnight. Pyridine adsorption took place at 150 °C for 20 min at a partial pressure of 800–1000 Pa, followed by desorption at 250 and 450 °C for 15 min. All spectra were recorded with a resolution of 2 cm<sup>-1</sup> by collecting 128 scans for a single spectrum. The extinction coefficients for pyridine adsorbed on Brønsted acid sites,  $\varepsilon(B) = 1.67 \text{ cm } \mu\text{mol}^{-1}$ , and Lewis acid sites,  $\varepsilon(L) = 2.22 \text{ cm } \mu\text{mol}^{-1}$ , were used for the quantitative analysis evaluation [34]. In a similar way, 2,6-di-*tert*-butyl pyridine was used as a probe molecule to assess the acidity of individual zeolites on their external surface, the adsorption was carried out at ambient temperature. The same extinction coefficient for Brønsted acid sites as for pyridine was used.

Nitrogen sorption isotherms were acquired at liquid nitrogen temperature (−196 °C) on a Micromeritics ASAP 2020 volumetric instrument to determine surface area, pore volume and pore size distribution of tested catalysts. Prior to the sorption measurements, all samples were degassed at 250 °C for at least 12 h.

### 2.4. Adsorption of 2,2-dimethylbutane

Kinetics of vapor phase adsorption of 2,2-dimethylbutane over zeolites at room temperature was studied using a Cahn C-2000 balance coupled with a computer via an ATI-Cahn digital interface (for details see Ref. [35]). 2,2-Dimethylbutane vapor was delivered from liquid 2,2-dimethylbutane with a 99.5% purity (Aldrich). The relative vapor pressure  $P/P_0$  was maintained at ~0.3 by controlling the temperature of the liquid adsorbate using a cooling circulator. Prior to the adsorption experiments, the calcined zeolites (~20 mg) were degassed at 450 °C in a vacuum of  $10^{-3}$  Torr for 5 h. The weight change of the zeolite sample was recorded for the 4 h of adsorption time. The adsorption capacities are reported in milliliters of liquid per gram of dry zeolite, assuming that the adsorbed adsorbate has the same density as the bulk liquid (0.649 g/ml for 2,2-dimethylbutane at room temperature).

### 2.5. Catalytic reactions

Toluene disproportionation and alkylation with isopropyl alcohol were investigated in the gas phase under atmospheric pressure using a glass fixed bed microreactor. Each catalyst was pressed into the pellets, crushed and sieved to obtain particles with a diameter in the range of 0.50–0.71 mm. Prior to the reaction, a given amount of the catalyst was in situ activated at 500 °C for 120 min in a stream of nitrogen (40 ml min<sup>-1</sup>), and then the activated catalyst was cooled down to the preset reaction temperature. In the case of toluene disproportionation, the reaction temperature was at 450 °C, WHSV 20 h<sup>-1</sup>, and the concentration of toluene in the feed stream using  $\text{N}_2$  as carrier gas was 18.5 mol%. Toluene alkylation was studied at the reaction temperature of 250 °C. The WHSV related to toluene was 10 h<sup>-1</sup>, the concentration of toluene was 18.5 mol% in the feed stream and toluene to isopropyl alcohol molar ratio was 9.6.

The reaction feeds and products were analyzed using an on-line gas chromatograph (HP 6890) equipped with an FID detector and a capillary column (DB-5, 50 m × 320  $\mu\text{m} \times 1 \mu\text{m}$ ) in toluene alkylation, while HP-INNOWax (30 m × 0.32 mm × 0.5  $\mu\text{m}$ ) was used for toluene disproportionation studies. The first sample was taken after 15 min of time-on-stream (T-O-S) and the other samples were taken in the interval of 60 min.

## 3. Results and discussion

### 3.1. Structural and textural characterization of zeolites under study

All zeolites under study were characterized by X-ray powder diffraction, scanning electron microscopy, adsorption isotherms and FTIR spectroscopy using pyridine and 2,6-di-*tert*-butyl pyridine as probe molecules. XRD patterns of zeolites TUN, IMF, −SVR, and \*SFV are provided in Fig. 2, while patterns of MFI and MEL are not shown here. All patterns exhibit typical features of these zeolites and evidence their phase purity and absence of amorphous phase.

The size and shape of zeolite crystals under study are given in Fig. 3. All zeolites, with exception of −SVR, show typical agglomerates of small crystals with sizes slightly below 1  $\mu\text{m}$  for MFI and MEL, around 0.4–0.6  $\mu\text{m}$  for \*SFV, IMF, and TUN. In contrast, zeolite −SVR forms crystals with a higher aspect ratio possessing some crystals up to 3  $\mu\text{m}$  long with smaller size of about 0.8  $\mu\text{m}$ .

Nitrogen adsorption isotherms are given in Fig. 4, while the textural properties of these zeolites are listed in Table 2. The isotherms of TUN, IMF, and −SVR exhibit very similar character including a substantial adsorption at low partial pressures followed by long

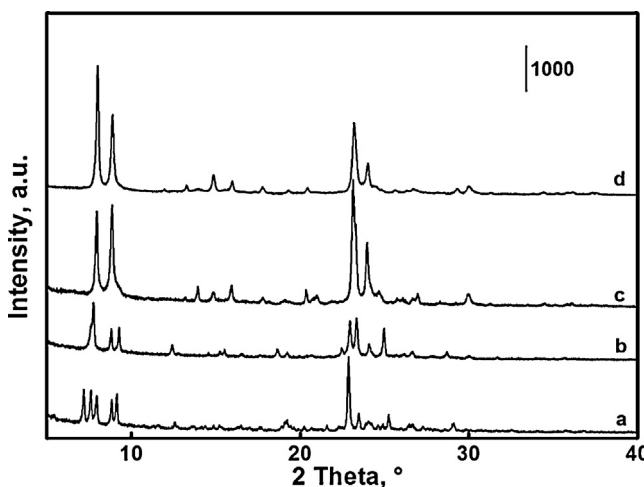


**Fig. 2.** XRD patterns of TUN (a), IMF (b), -SVR (c), \*SFV (d).

**Table 2**

Textural and chemical properties of zeolites under study.

Sample	BET (m <sup>2</sup> /g)	V <sub>mic</sub> (cm <sup>3</sup> /g)	V <sub>tot</sub> (cm <sup>3</sup> /g)	Si/Al (XRF)
TUN	381	0.167	0.194	19.5
IMF	331	0.136	0.177	33.8
-SVR	328	0.130	0.210	105
SFV	402	0.144	0.449	40.0
MFI	423	0.160	0.252	34.5
MEL	298	0.147	0.200	33.0

plateau up to  $P/P_0$  equal to 0.95. Very little adsorption in interparticle space is visible at higher pressures. In contrast, \*SFV shows a substantial increase in the adsorbed amount at pressures higher than 0.6. This adsorption feature is characteristic for interparticle adsorption in aggregates with a large free volume being in this zeolite around 0.3 cm<sup>3</sup>/g. Micropore volumes of all zeolites under study are between 0.130 and 0.167 cm<sup>3</sup>/g, confirming a high crystallinity and phase purity of these zeolites (Table 2).

### 3.2. Acidity study: concentration and strength of the acid sites

The acidity of novel zeolites TUN, IMF, -SVR, and \*SFV as well as reference samples (MFI and MEL) was investigated by adsorption of pyridine (kinetic diameter 0.5 nm) and 2,6-di-*tert*-butyl pyridine (kinetic diameter 0.7 nm), which is not able to penetrate to the 10-ring channels of these zeolites. After activation in vacuum, pyridine

was adsorbed in excess at 150 °C and then desorbed at the temperature of 250 °C for 20 min to remove the gas phase and weakly bonded species. Further on, desorption of pyridine was also carried out at 450 °C. The reason for choosing these temperatures was that alkylation reaction was performed at 250 °C, while the disproportionation at 450 °C. Although pyridine was used as probe molecule for acidity assessment and not toluene, due to its reactivity, we tried to correlate the activity to the number of acid sites recorded at the reaction temperatures.

Concentrations of Brønsted and Lewis sites were determined from the intensities of the IR bands of protonated and coordinatively bonded pyridine [34] (Table 3). FTIR spectra of adsorbed pyridine before and after desorption at 250 and 450 °C are given in Figs. 5 and 6. Hydroxyl group region of FTIR spectra of all zeolites under study consists of absorption bands of silanol groups around 3742 cm<sup>-1</sup> and bands of bridging OH groups around 3610–3620 cm<sup>-1</sup>. In the case of TUN and IMF, we observed also a low intensity band around 3665 cm<sup>-1</sup> being typical of Al–OH vibrations. The only difference is the spectrum of hydroxyl region of zeolite -SVR. In this spectrum (Fig. 5), we found an additional absorption around 3720 cm<sup>-1</sup>. This band can be assigned to silanol groups located in this zeolite. This is characteristic feature for -SVR zeolite possessing one empty site in the unit cell. While there are 24 crystallographically different T-sites in the unit cell of -SVR, only 23 of them are occupied by Si or Al atoms [14].

All zeolites under study show higher concentrations of Brønsted acid sites than Lewis acid sites. The decreasing order of concentrations of Brønsted acid sites determined from pyridine desorption at 250 °C is as follows TUN > IMF ≈ MEL > MFI ≈ \*SFV > -SVR (Table 3). The maximum concentrations of Lewis acids sites reached only 0.10 mmol/g and they decreased in the following order IMF > TUN ≈ MEL ≈ \*SFV > -SVR ≈ MFI. These values will be related in the catalytic part to conversions and selectivities in toluene alkylation with isopropyl alcohol.

Concentrations of Brønsted and Lewis acid sites were also determined after pyridine desorption at 450 °C and these values will be related to toluene disproportionation. Table 3 evidences a substantial decrease in the concentrations of Brønsted acid sites titrated by pyridine between 250 and 450 °C while concentrations of Lewis acid sites decreased less. The only exception was found for MEL zeolite. The concentration of Brønsted acid sites for MEL decreased only from 0.21 to 0.19 mmol/g between 250 and 450 °C evidencing high stability of acid sites of MEL zeolite at this temperature.

2,6-Di-*tert*-butyl pyridine (DTBP) was used as a probe molecule to titrate the external surface of zeolite crystals under study [36]. Adsorption of DTBP on Brønsted acid sites gives rise to a new absorption band around 1530 cm<sup>-1</sup> (Figs. 7 and 8). The absence of the absorption band at 1545 cm<sup>-1</sup> evidences that *tert*-butyl groups

**Table 3**

Concentration of Lewis and Brønsted acid sites on zeolites studied.

Zeolite	Desorption temp. °C	c <sub>Al</sub> (mmol/g)	c <sub>Br</sub> (mmol/g)	c <sub>Le</sub> (mmol/g)	c <sub>Br</sub> (%)	c <sub>Le</sub> (%)	c <sub>Br</sub> (*) (mmol/g)
TUN	250	0.63	0.48	0.07	87	13	<0.01
	450	0.42	0.27	0.07	79	21	
IMF	250	0.45	0.23	0.10	70	30	0.02
	450	0.27	0.12	0.08	60	40	
-SVR	250	0.13	0.05	0.04	56	44	0.02
	450	0.05	0.01	0.02	33	67	
MFI	250	0.22	0.15	0.03	83	17	0.02
	450	0.13	0.08	0.02	80	20	
MEL	250	0.33	0.21	0.06	78	22	0.02
	450	0.30	0.19	0.05	79	21	
SFV	250	0.26	0.15	0.06	71	29	0.04
	450	0.19	0.09	0.05	64	36	

c<sub>Al</sub> – concentration of Al, c<sub>Br</sub> – concentration of Brønsted acid sites; c<sub>Le</sub> – concentration of Lewis acid sites; c<sub>Br</sub><sup>\*</sup> – concentration of Brønsted acid sites determined from 2,6-di-*tert*-butylpyridine adsorption.

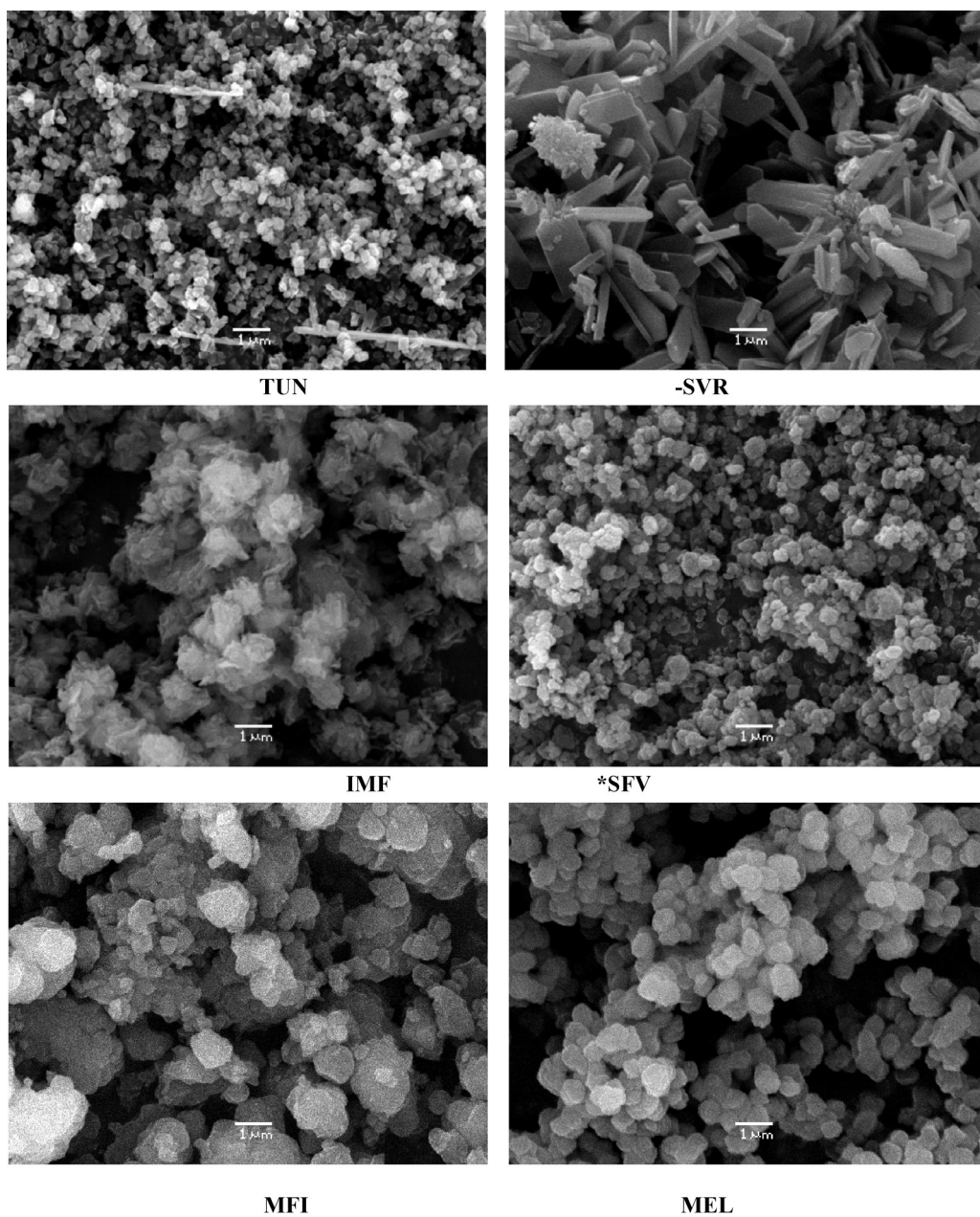


**Fig. 3.** SEM images of zeolites under investigation.

remained at pyridine and no dealkylation proceeded during the adsorption experiment. The values of Brønsted acid sites located on the external surface of zeolite crystals are rather low and usually around 0.02 mmol/g being even less for TUN zeolite (cf. Table 3).

### 3.3. Adsorption of 2,2-dimethylbutane

Kinetics of vapor phase adsorption of 2,2-dimethylbutane was investigated at room temperature [35]. The results show that the diffusivity of 2,2-dimethyl butane in this series of zeolite differing in the sizes of their channel entrances decreases systematically with the decreasing diameter of the channels. The fastest uptake is clearly visible for TUN zeolite (Fig. 9) followed by \*SFV. The structure of \*SFV consists of large parts of crystals formed by MEL structure, in addition with a portion of part possessing 12-ring channel. Similar kinetics of 2,2-dimethyl butane adsorption was found for zeolites IMF and -SVR, followed by MFI and MEL. This

order of diffusion rates shows the increasing hindrances among individual zeolites based on their different sizes of the channel entrance windows.

### 3.4. Toluene alkylation with isopropyl alcohol

Toluene alkylation with isopropyl alcohol provides *o*- and *p*-cymenes as primary alkylation products and selectivity to *p*-cymene is controlled by diffusion of individual isomers inside the channel system of the respective zeolite. Generally, with increasing pore size, composition of cymenes is closer to the thermodynamic one while for MFI zeolite, high *para*-selectivity is usually obtained [37].

Zeolites studied can be divided according to their conversions in toluene alkylation with isopropyl alcohol into several groups related to their structures. TUN exhibited the highest toluene conversion of about 9% after 15 min of T-O-S due to a contribution of

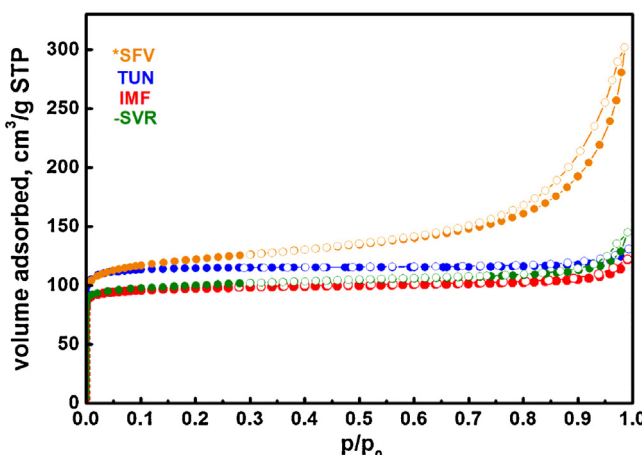


**Fig. 4.** Nitrogen adsorption (●)/desorption (○) isotherms of zeolites of TUN, IMF, -SVR, \*SFV.

toluene disproportionation. IMF, and -SVR exhibited toluene conversions around 7% stable in time (reaction temperature 250 °C, toluene/isopropyl alcohol molar ratio 9.6 h<sup>-1</sup>). In contrast, MFI, MEL, and \*SFV reached toluene conversions close to 5%. Size of the zeolite channels is the main feature distinguishing the structural properties of both these groups of zeolites. While MFI, MEL, and \*SFV possess the channel size of about 0.55 nm (with exception of

relatively low amount (1/15) of 12-rings in the case of \*SFV), the size of zeolite channels of TUN, IMF, and -SVR is close to 0.6 nm. This difference seems to be decisive for higher toluene conversions of the latter group of zeolite catalysts.

Overall selectivity to cymenes is also related to differences in structural features of zeolites investigated. MFI, MEL (around 50%), and at some extent also \*SFV (60%) exhibit relatively low selectivities to cymenes due to the formation of *n*-propyltoluenes in the second reaction step [38]. Selectivity to cymenes over TUN and IMF increased from about 30–40% after 15 min of T-O-S to about 80% after 180 min. It indicates that there are some accessible channel intersections, in which the bimolecular transformations of cymenes to *n*-propyltoluenes proceeds and these sites are probably deactivated in the first stages of the reaction. In contrast, almost 90% of cymenes are formed during the whole kinetic run over -SVR zeolite.

Selectivities to cymenes and *n*-propyltoluenes can be also presented as *iso*-/*n*-propyltoluene ratios (Fig. 10). MFI and MEL zeolites are well-known for their low *iso*-/*n*-ratios between 1 and 2 [39]. Zeolite \*SFV exhibited almost constant conversion with T-O-S reaching the value around 3. This indicates that there is a significant amount of channel intersections in \*SFV being rather close similar to the intersections in MFI and MEL zeolites. It is fully consistent with the structure of \*SFV zeolite possessing large part of the crystals with MEL structure [15]. As described about cymene selectivities, *iso*-/*n*- ratio increased from 1 to about 10–11 for TUN and IMF within the first 180 min of the reaction. -SVR exhibited constant *iso*-/*n*- ratio during the whole kinetic experiment.

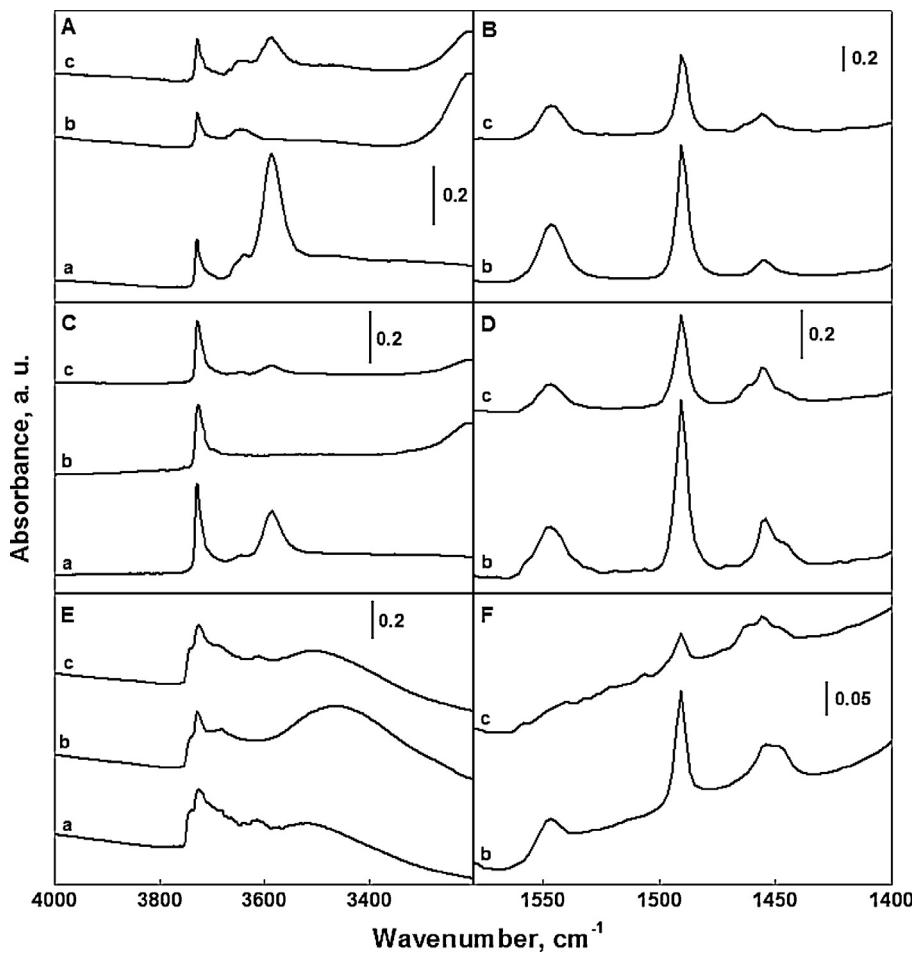


**Fig. 5.** IR spectra of pyridine adsorption/desorption over TUN (A, B), IMF (C, D) and. -SVR (E, F) zeolites; A, C, E – region of hydroxyl vibration; B, D, F – region of acid sites. (a) before adsorption, (b) after desorption at 250 °C, (c) after desorption at 450 °C

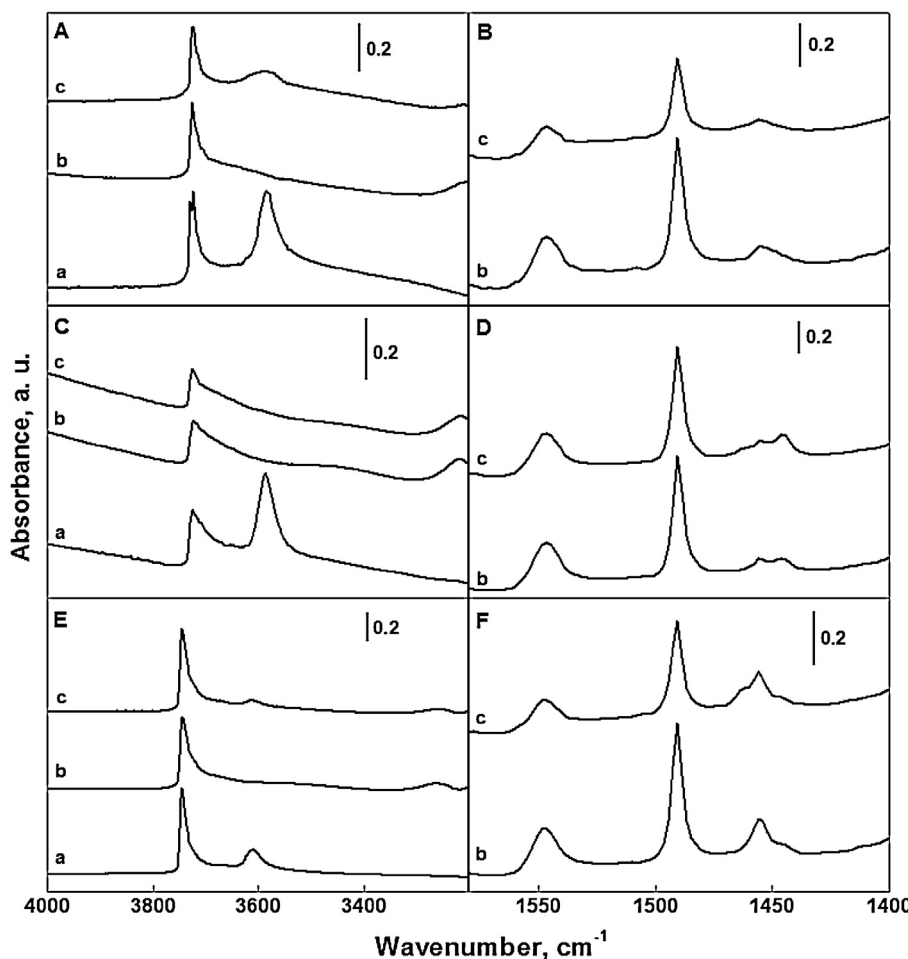


**Fig. 6.** IR spectra of pyridine adsorption/desorption over MFI (A, B), MEL (C, D) and \*SFV (E, F) zeolites; A, C, E – region of hydroxyl vibration; B, D, F – region of acid sites. (a) Before adsorption, (b) after desorption at 250 °C, (c) after desorption at 450 °C.

Selectivities to *p*-cymene reflect again the structural features of zeolites under study. Selectivity to *para*-isomers is strongly related to the diffusion of individual cymene isomers through the channel systems of these zeolites. MFI and MEL exhibited very similar *p*-

cymene selectivities reaching around 75% after 180 min of T-O-S. Zeolite -SVR provided constant *p*-cymene selectivity close to 62%. This is probably due to low concentration of acid sites and *p*-cymene is formed as primary product with *o*-cymene. The most intriguing

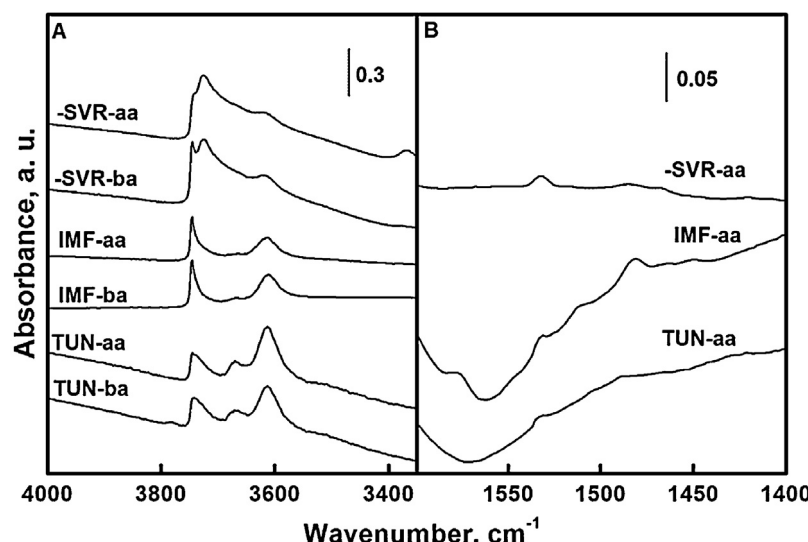


**Fig. 7.** IR spectra of DTBP adsorption/desorption over TUN, IMF and -SVR zeolites; (A) region of hydroxyl vibration; (B) region of acid sites, before (ba) and after (aa) adsorption.

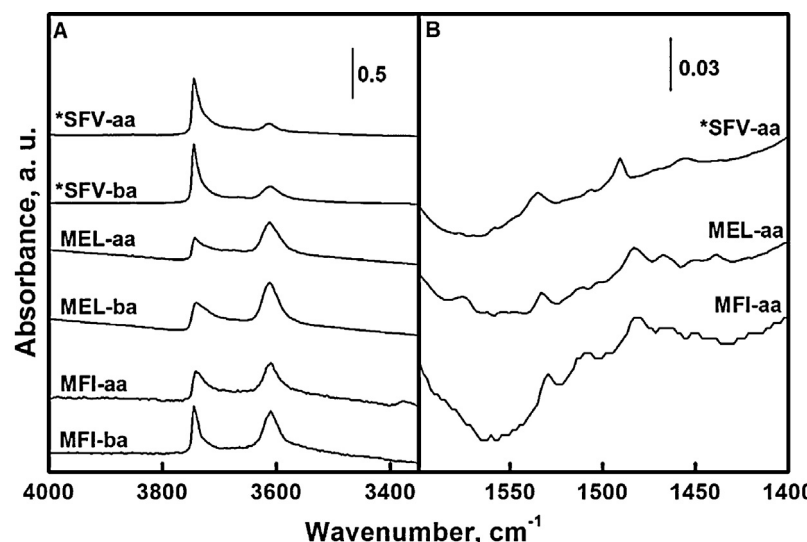


**Fig. 8.** IR spectra of DTBP adsorption/desorption over MFI, MEL and \*SFV zeolites; (A) region of hydroxyl vibration; (B) region of acid sites, before (ba) and after (aa) adsorption.

is low selectivity to *p*-cymene over \*SFV zeolite achieving 50% after 180 min of T-O-S. Lower *p*-cymene selectivity was obtained only over TUN zeolite.

Desorption of cymenes and their transport were recognized as the rate limiting steps of toluene alkylation with isopropyl alcohol over zeolites [39]. This fact strongly diminishes the role of type and concentration of acid sites in 10-ring zeolites on the resulting toluene conversions. As reported for other zeolites [34] toluene conversions follow the size of the channels and not the acidity. In our case, the highest concentrations of Brønsted acid sites and overall concentrations of acid sites are in the order TUN > IMF > MEL > MFI ≈ \*SFV > -SVR. However, the order of toluene conversions after 60 min of T-O-S is -SVR > IMF > TUN > \*SFV ≈ MEL > MFI. This order can be straightforwardly related neither to the concentration of acid sites nor to the size of the individual zeolite crystals.

### 3.5. Toluene disproportionation

Larger channel entrances of zeolites TUN and IMF play a dominant role also as for the toluene conversion in toluene disproportionation performed at 450 °C. WHSV equal to 20 h<sup>-1</sup> was

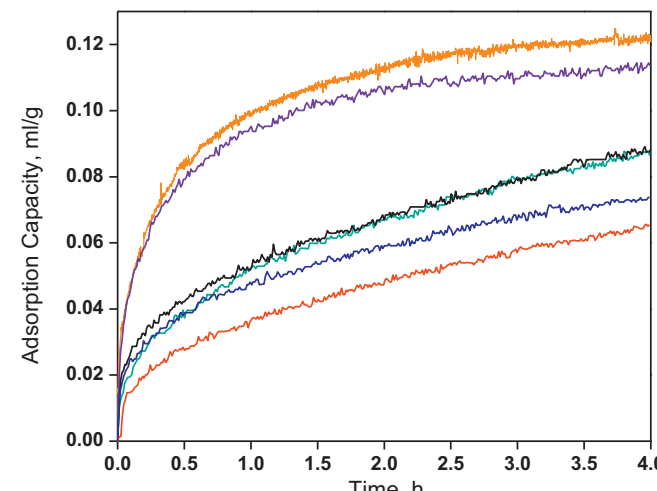


**Fig. 9.** Kinetics of adsorption of 2,2-dimethylbutane over zeolites under study (■ TUN, ■ -SVR, ■ \*SFV, ■ IMF, ■ MEL, ■ MFI).

used to differentiate differences in toluene conversion over zeolites studied (see Fig. 11). The initial conversion over TUN zeolite is about 40% while for IMF around 15%. Toluene conversions over other zeolites studied are less than 5%. Again, toluene conversion are in a good agreement with the sizes of channel entrances of 10-ring zeolites in the order of TUN > IMF > \*SFV > MFI > MEL > -SVR.

Similar structural features of 10-ring zeolites are responsible to similar selectivities to xylenes reaching around 45%. It is seen that toluene disproportionation is dominant reaction under the conditions used as the molar ratio of both primary products (benzene/xylene) is above 0.9. Although it should be noted that toluene conversions achieved were rather low for MFI, MEL, and -SVR zeolites. Significant differences can be seen in selectivities to *p*-xylene when comparing different structural types of zeolites. Similarly to selectivity to *p*-cymene in toluene alkylation with isopropyl alcohol, \*SFV again exhibited low selectivity to *p*-xylene similar to MFI and TUN zeolites reaching practically thermodynamic equilibrium values.

In contrast to toluene alkylation with isopropyl alcohol, toluene conversions in its disproportionation are much more related to the both size of the channels and concentrations of acid sites. The highest toluene conversions were reached over TUN and IMF zeolites, those having the most open structures but also the highest concentrations of acid sites (Table 3). In opposite, the lowest conversion was obtained over -SVR, the zeolite with the minimum concentration of acid sites, despite relatively open 10-ring channel structure.

### 3.6. Assessment of structure–activity–selectivity relationship

The following characteristic features were obtained in 2,2-dimethylbutane adsorption, toluene disproportionation and toluene alkylation with isopropylalcohol over a series of 10-ring zeolites TUN, IMF, \*SFV, MFI, MEL, and -SVR:

- (1) The highest initial rates of adsorption were obtained for TUN, and \*SFV. While in the case of TUN this result was expected due to larger pore entrances than in MFI and MEL zeolites. With \*SFV, although most of its structure consisting of MEL zeolite, a small portion of its structure consists of 12-rings and contributes to its quick initial adsorption rate.
- (2) Toluene conversions in toluene disproportionation showed a large difference between TUN and IMF zeolites and the remaining zeolites. This can be explained in terms of larger

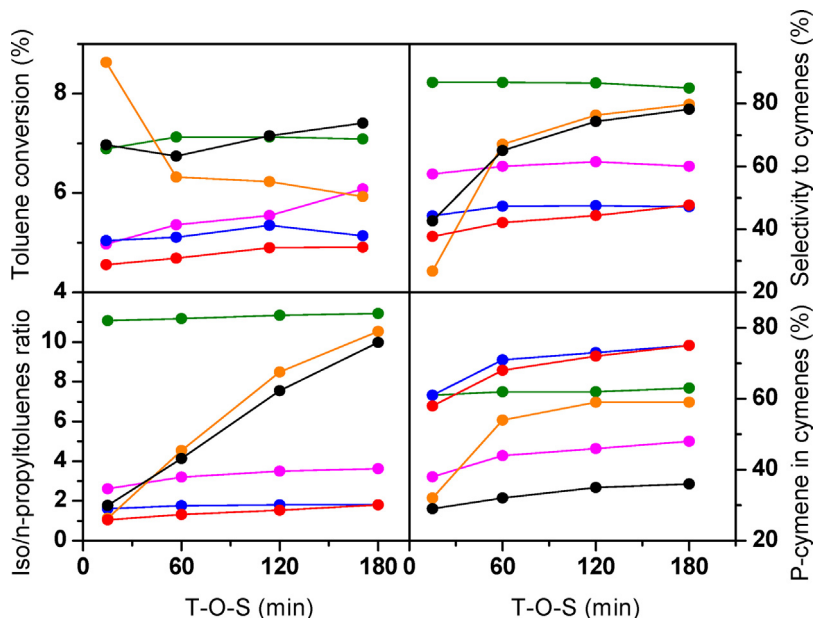


**Fig. 10.** Time-on-stream dependences of toluene conversions and selectivities to cymenes, *p*-cymene and *iso*-/n-propyl toluenes over zeolites studied (■ TUN, ■ -SVR, ■ \*SFV, ■ IMF, ■ MEL, ■ MFI).

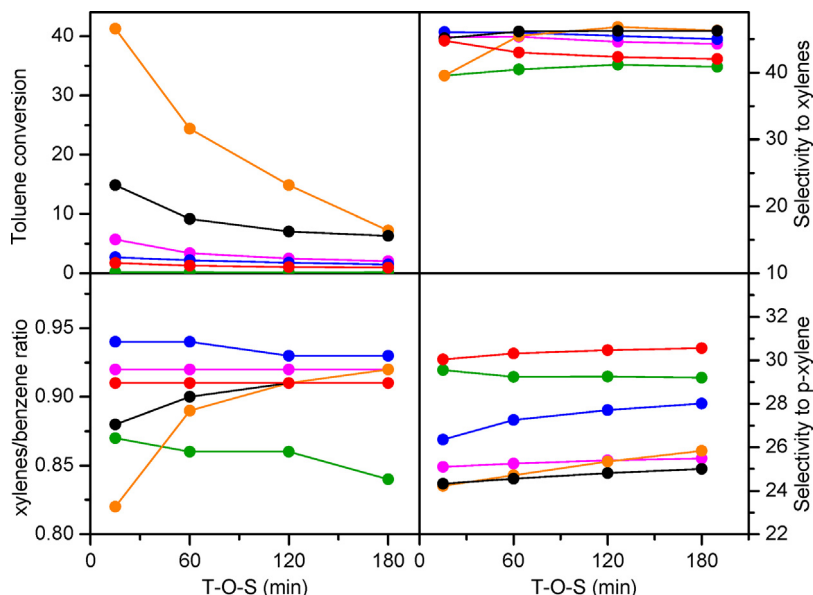


**Fig. 11.** Time-on-stream dependences of toluene conversions and selectivities to xylenes, *p*-xylene and benzene/toluene ratio in toluene disproportionation over zeolites studied (■ TUN, ■ -SVR, ■ \*SFV, ■ IMF, ■ MEL, ■ MFI).

- pores of TUN and IMF and higher concentration of acid sites when compared with zeolite -SVR.
- (3) Toluene conversions in toluene alkylation distinguished again zeolites into two groups - TUN, IMF, and -SVR exhibited higher conversion than \*SFV, MFI, and MEL, which can be explained by different pore sizes (cf. Table 1).
  - (4) Zeolites \*SFV, MFI, and MEL exhibit similar selectivities to *n*-propyltoluenes confirming the same (similar) reaction space at channel intersections for cymene bimolecular reaction with toluene.
  - (5) \*SFV zeolite exhibits not only high rate of 2,2-dimethylbutane adsorption but also low selectivity to *p*-xylene and *p*-cymene. These results evidence that transport of molecules is less restricted in the channel system (or at least in a part of it) of \*SFV zeolite compared with MFI or MEL.

Because of part of the structure of \*SFV crystals consists of MEL structure, the differences in adsorption and selectivities should be related to the presence of 12-ring channels. High concentrations of *n*-propyltoluenes formed evidence on one hand side that the bimolecular reaction proceeds in MEL channel intersections, on the other side high selectivities to *n*-propyltoluenes could be due to a minimum amount of active sites in 12-ring channels.

#### 4. Conclusions

Zeolites with three-dimensional 10-ring channel systems, namely, TUN, IMF, \*SFV, MFI, MEL, and -SVR, were evaluated for their catalytic and adsorption properties using 2,2-dimethyl butane adsorption, toluene disproportionation and toluene alkylation with isopropyl alcohol. It was found that differences in pore sizes of

about 0.03–0.04 nm play important role in toluene conversions and selectivities to *n*-propyltoluenes and *para*-selectivities.

TUN, IMF, and –SVR with pore sizes close to 0.6 nm exhibited higher conversion and lower *para*-selectivities compared with MFI and MEL zeolites with pore sizes around 0.55 nm.

The pore size differences were also clearly evidenced in selectivities to *n*-propyltoluenes formed by consecutive bimolecular reaction between primary formed cymenes and toluene. *Iso-/n*-propyltoluene ratio over zeolites \*SFV, MFI, and MEL reached values 1.5–2.0 confirming the effect of the size of channel intersections on the mechanism of *n*-propyltoluene formation.

Expectedly, MFI and MEL zeolites exhibited the highest selectivity to *para*-isomers while \*SFV exhibited low *para*-selectivity and high adsorption rate for 2,2-dimethylbutane. As the large part of the crystals of \*SFV consist of MEL structure it is proposed that 12-ring channels play a dominant role in transport of reactants and products in \*SFV zeolite.

## Acknowledgements

This work was supported by the Czech Science Foundation Grant No. P106/12/G015 (Center of Excellence). SAK acknowledges the Ministry of Higher Education of Saudi Arabia for establishing the Center of Research Excellence in Petroleum Refining and Petrochemicals at KFUPM.

## References

- [1] W.W. Kaeding, G.C. Barile, M.M. Wu, *Catal. Rev.-Sci. Eng.* 26 (1984) 597–612.
- [2] S. Al-Khattaf, S.A. Ali, A.M. Aitani, N. Zilkova, D. Kubicka, J. Čejka, *Catal. Rev.-Sci. Eng.* 56 (2014) 333–402.
- [3] T. Odedairo, S. Al-Khattaf, *Chem. Eng. J.* 167 (2011) 240–254.
- [4] C. Perego, P. Ingallina, *Catal. Today* 73 (2002) 3–22.
- [5] T.C. Tsai, S.B. Liu, I.K. Wang, *Appl. Catal. A: Gen.* 181 (1999) 355–398.
- [6] J. Čejka, G.A. Kapustin, B. Wichterlova, *Appl. Catal. A: Gen.* 108 (1994) 187–204.
- [7] J. Čejka, A. Vondrova, B. Wichterlova, G. Vorbeck, R. Fricke, *Zeolites* 14 (1994) 147–153.
- [8] A. Corma, V.I. Costa-Vaya, M.J. Diaz-Cabanas, F.J. Llopis, *J. Catal.* 207 (2002) 46–56.
- [9] A. Corma, F.J. Llopis, C. Martinez, G. Sastre, S. Valencia, *J. Catal.* 268 (2009) 9–17.
- [10] F.J. Llopis, G. Sastre, A. Corma, *J. Catal.* 242 (2006) 195–206.
- [11] <http://www.iza-online.org/> (accessed 14.05.15).
- [12] S.I. Zones, C.Y. Chen, A. Corma, M.T. Cheng, C.L. Kirby, I.Y. Chan, A.W. Burton, *J. Catal.* 250 (2007) 41–54.
- [13] M. Moliner, M.J. Diaz-Cabanas, V. Fornes, C. Martinez, A. Corma, *J. Catal.* 254 (2008) 101–109.
- [14] R.E. Morris, J. Čejka, *Nat. Chem.* 7 (2015) 381–388.
- [15] P. Eliášová, M. Opanasenko, P.S. Wheatley, M. Shamzhy, M. Mazur, P. Nachtigall, W.J. Roth, R.E. Morris, J. Čejka, *Chem. Soc. Rev.* (2015), <http://dx.doi.org/10.1039/c5cs00045a>
- [16] A. Corma, *Chem. Rev.* 95 (1995) 559–614.
- [17] S.I. Zones, C.Y. Chen, A. Benin, S.J. Hwang, *J. Catal.* 308 (2013) 213–225.
- [18] R. Millini, G. Perego, W.O. Parker Jr., G. Bellussi, L. Carluccio, *Microporous Mater.* 4 (1995) 221–230.
- [19] M. Choi, K. Na, J. Kim, Y. Sakamoto, O. Terasaki, R. Ryoo, *Nature* 461 (2009) 246–U120.
- [20] P. Chlubna, W.J. Roth, H.F. Greer, W.Z. Zhou, O. Shvets, A. Zukal, J. Čejka, R.E. Morris, *Chem. Mater.* 25 (2013) 542–547.
- [21] A. Corma, V. Fornes, S.B. Pergher, T.L.M. Maesen, J.G. Buglass, *Nature* 396 (1998) 353–356.
- [22] W.J. Roth, *Stud. Surf. Sci. Catal.* 158 (2005) 19–26.
- [23] X.Y. Zhang, D.X. Liu, D.D. Xu, S. Asahina, K.A. Cychosz, K.V. Agrawal, Y. Al Wahedi, A. Bhan, S. Al Hashimi, O. Terasaki, M. Thommes, M. Tsapatsis, *Science* 336 (2012) 1684–1687.
- [24] M. Milina, S. Mitchell, N.L. Michels, J. Kenvin, J. Perez-Ramirez, *J. Catal.* 308 (2013) 398–407.
- [25] J. Perez-Ramirez, C.H. Christensen, K. Egeblad, C.H. Christensen, J.C. Groen, *Chem. Soc. Rev.* 37 (2008) 2530–2542.
- [26] C. Jo, J. Jung, R. Ryoo, *Microporous Mesoporous Mater.* 194 (2014) 83–89.
- [27] S.B. Hong, H.K. Min, C.H. Shin, P.A. Cox, S.J. Warrender, P.A. Wright, *J. Am. Chem. Soc.* 129 (2007) 10870–10885.
- [28] C. Baerlocher, F. Gramm, L. Massuger, L.B. McCusker, Z.B. He, S. Hovmoller, X.D. Zou, *Science* 315 (2007) 1113–1116.
- [29] C. Baerlocher, D. Xie, L.B. McCusker, S.J. Hwang, I.Y. Chan, K. Ong, A.W. Burton, S.I. Zones, *Nat. Mater.* 8 (2008) 631–635.
- [30] E. Benazzi, J.L. Guth, L. Rouleau, *PCT WO 98/17581*, 1998.
- [31] A. Corma, A. Chica, J.M. Gui, F.J. Llopis, G. Mabilon, J.A. Perdigon-Melon, S. Valencia, *J. Catal.* 189 (2000) 382–394.
- [32] S.I. Zones, A.W. Burton, K. Ong, US 2007/0148086 A1, 2007.
- [33] S.A. Elomari, US Patent 6,544,495, 2003.
- [34] N. Zilkova, M. Bejblova, B. Gil, S.I. Zones, A.W. Burton, C.Y. Chen, Z. Musilova-Pavlackova, G. Kosova, J. Čejka, *J. Catal.* 266 (2009) 79–91.
- [35] C.Y. Chen, S.I. Zones, *Microporous Mesoporous Mater.* 104 (2007) 39–45.
- [36] A. Corma, V. Fornes, L. Forni, F. Marquez, J. Martinez-Triguero, D. Moscotti, *J. Catal.* 179 (1998) 451–458.
- [37] C. Jo, R. Ryoo, N. Zilkova, D. Vitvarova, J. Čejka, *Catal. Sci. Technol.* 3 (2013) 2119–2129.
- [38] B. Wichterlova, J. Čejka, N. Zilkova, *Microporous Mater.* 6 (1996) 405–414.
- [39] B. Wichterlova, J. Čejka, *J. Catal.* 146 (1994) 523–529.